Journal of Colloid and Interface Science 584 (2021) 789–794

Contents lists available at ScienceDirect

Journal of Colloid and Interface Science

journal homepage: www.elsevier.com/locate/jcis

Regular Article

Thermally-driven gold@poly(*N*-isopropylacrylamide) core-shell nanotransporters for molecular extraction

Chi Zhang [1], Fangfang Deng [1], Wenqi Xiong, Xujie Wang, Shengjun Yuan, Tao Ding

Key Laboratory of Artificial Micro- and Nano-structures of Ministry of Education of China, School of Physics and Technology, Wuhan University, Wuhan 430072 China

GRAPHICAL ABSTRACT

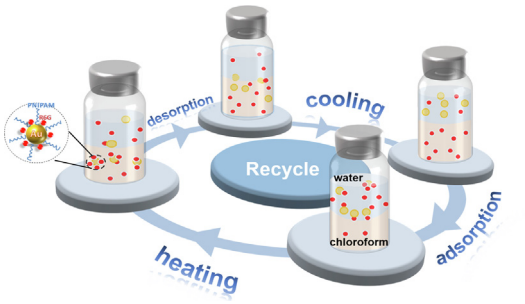

ARTICLE INFO

Article history:
Received 14 August 2020
Revised 17 September 2020
Accepted 3 October 2020
Available online 13 October 2020

Keywords:
Extraction
Gold nanoparticles
Extinction
Nanotransporters

ABSTRACT

Hypothesis: Molecular extraction efficiency can be boosted with the assistance of nanoparticles (NPs). It is based on adsorption of the extractants in one phase and desorption in another phase, which requires a reversible phase transfer of the NPs.

Experiments: We synthesized the gold@poly(*N*-isopropylacryamide) (Au@PNIPAM) NPs via an interfacial self-assembly method enhanced by post-polymerization. We adopted Rhodamine 6G (R6G) as the model molecule for the extraction test. In comparison, UV–Vis extinction spectra were recorded to monitor the extraction processes with or without the Au@PNIPAM NPs. We further analyzed theoretically with thermodynamics and first-principle calculations.

Findings: The hybrid Au@PNIPAM NPs show a reversible phase transfer between the interface and chloroform phases. The Au NPs assisted extraction efficiency of R6G shows 5 times higher than that without Au NPs. The thermodynamic analysis of the nanotransportation system agrees well with the *ab initio* density functional theory calculations. This nanoparticle-assisted molecular transportation modifies the extraction kinetics significantly, which will provide further implications for biphasic catalysis, pollutant treatment and drug delivery.

1. Introduction

Extraction techniques, including both liquid-liquid and solid-liquid extraction, play a very important role in chemical and environmental engineering [1]. Conventional extraction efficiency is related to the distribution coefficient of the extracts in two phases, which is determined by the thermodynamics [2]. To improve the extraction efficiency, it is essential that the thermodynamic energy landscape of the extraction system is modified, which leads to the invention of advanced extraction techniques, such as partition of aqueous two-phase systems, reverse micelle extraction, and supercritical fluid extraction (SCF) [3–8].

[1] These two authors contributed equally to this work.

E-mail address: t.ding@whu.edu.cn (T. Ding)

https://doi.org/10.1016/j.jcis.2020.10.008
0021-9797/

Nanoparticle-mediated solvent extraction provides another promising opportunity towards efficient extraction. This extraction mechanism is mostly based on absorption and desorption of the extracts on the nanoparticles, which is actually a liquid-solid extraction [9,10]. However, their release from the nanoparticles becomes a problem if the extracts have a strong affinity to the nanoparticles. Moreover, most of the nanoparticle extractants are not reversible and recyclable, which increases the cost. Although this recyclability issue can be resolved by using magnetic particles for extraction, it is only applicable for certain types of molecules and vulnerable to acid condition [11].

Metallic nanoparticles such as gold are stable in many solvents with high surface to volume ratio, which can be an effective adsorber for most organic molecules. It also provides an opportunity to monitor the extraction process due to its plasmonic absorbance for the visible light. However, due to the limitation of their synthetic conditions, they are either born hydrophilic or hydrophobic, making them not a good candidate for molecular extraction. Although surface functionalization can transfer the gold nanoparticles (Au NPs) into the other phase, they are mostly not reversible and the ligandation on the surfaces causes limited accessibility for the extracts [12–20].

Poly(*N*-isopropylacrylamide) (PNIPAM), which contains both polar and nonpolar segments in the polymer chains, shows some amphiphilic property [21]. Moreover, it has a lower critical solution temperature (LCST), above which it changes its surface hydrophobicity, rendering reversible phase transfer [22]. Unlike small molecule ligands, PNIPAM has a fairly low grafting density on Au NPs [23], which leaves many of vacancy on the surface of Au NPs for the extracts' adsorption. With these advantages, we propose a nanoparticle-assisted solvent extraction system that is based on the reversible phase transfer of Au@PNIPAM hybrid NPs. The temperature responsive PNIPAM aids the reversible phase transfer of Au NPs between water and chloroform ($CHCl_3$) upon heating and cooling. During the phase transfer, the model molecules (Rhodamine 6G, R6G) in aqueous phase adsorbed on Au NPs are transported into the $CHCl_3$ phase during the heating cycle, which are subsequently released via desorption from the surface of Au NPs. Interestingly, these Au NPs can go back to the water/$CHCl_3$ interface after cooling the temperature below the LCST, which reloads the R6G molecules for the next round of transportation. We further explain this nanotransportation process from the perspective of thermodynamics and kinetics. This concept of nanotransportation not only enriches the family of colloidal machines [24], but also suggests potential applications for pollutants removal, targeted delivery, and biphasic catalysis [25–28].

2. Materials and methods

2.1. Preparation of the nano-transport system and characterizations

The Au NPs were synthesized according to Turkevich's method [29]. Typically, 34.94 mg of trisodium citrate (99.9%, Acros organics) dihydrate was dissolved in 149 mL water under magnetic stirring, which was refluxed at 100 °C for 15 mins. Then 1 mL of 32.8 mM aqueous solution of gold (III) chloride trihydrate (≥99.9% trace metal basis, Sigma-Aldrich) was quickly injected into the solution for burst nucleation and growth of Au NPs. The Au NPs were harvested after refluxing the solution for 2 hrs [30]. Their optical properties were characterized with UV–Vis extinction spectra recorded with optifiber spectrometer (QE65000, Ocean Optics), see supporting information (SI) Fig. S1a. The hydrodynamic diameter of the as-synthesized Au NPs is 17 ± 2 nm (SI-Fig. S1b) as determined by Zetasizer (Malvern). Scanning electron microscope (SEM, Zeiss SIGMA) image of the Au NPs further confirms their actual size is 13 ± 2 nm (SI-Fig. S1c). The slight discrepancy from hydrodynamic diameter is reasonably expected due to the existence of ligands in solution.

To prepare the Au/PNIPAM phase transfer system, 1 mL of the as-synthesized Au NPs was mixed with 2 μL PNIPAM-SHCOOH (10 mg/mL, M_w = 6000, PDI ≤ 1.2 from Sigma-Aldrich) and incubated at 40 ℃ for 5 mins. 20 μL of NaCl aqueous solution (1 M, 99.8%, Macklin) and 1 mL chloroform (99%, Yonghua Chemical CO., LTD) were consequently added to form a biphasic system (Fig. 1a). Centrifugation (~10 k g, 10 min) was applied to this biphasic liquids, which led to the precipitation of Au NPs to the oil and water interface [16]. The aqueous phase was then withdrawn into a small droplet with volume of ~20 μL. To enhance the PNIPAM coating, a 10 μL NIPAM monomer solution (99%, 2 M, Acros organics) containing initiator (100 μg $K_2S_2O_8$, ≥99.5%, Adamas-beta) was injected to the droplet for further polymerization (60 °C, 30 min). The hydrodynamic diameter of Au@PNIPAM core-shell NPs is increased from 19 to 23 nm after this post-polymerization (SI-Fig. S2). The reversible phase transfer behaviour of Au NP@PNIPAM was characterized by monitoring the UV–Vis spectra of Au NPs in oil phase (Chloroform) by cycling the temperature between 25 and 45 °C. Dark field and transmission optical images of the plasmonic microemulsion were captured with 10×/20× objective (Olympus). The Au@PNIPAM core-shell NPs were further characterized with the transmission electron microscope (TEM, JEM-2010HT) at the accelerating voltage of 200 kV.

2.2. Extraction of R6G with metallic nanotransporters

10 μL of R6G (99%, Acros organics) solution (6.9 mM) was injected into the water droplet containing AuNP@PNIPAM. Heating and cooling (with ramping rate of 10 °C/min) of the system for several cycles led to the extraction of R6G from water into chloroform. A control experiment without Au NPs was performed in the same way. The heating and cooling of the solution was implemented in a qpod-2e setup (Quantum Northwest), which allows simultaneous recording of the UV–Vis spectra during the extraction process. The concentration of R6G in chloroform and water were calibrated with standard correlation between concentration and absorbance based on Lambert-Beer law (SI-Fig. S3).

2.3. First-principle calculations

The first-principle calculations are carried out by the VASP package based density functional theory (DFT), in which the electron-ion potential and exchange-correlation functional are treated by the generalized gradient approximation (GGA) and projected augmented wave (PAW) [31]. For the structural relaxations, the kinetic energy cutoff is set to 400 eV. The vacuum region of 20 Å is used to avoid the periodic interaction. The complex system contains double Au atomic layer, 1 R6G molecule, 25 H_2O molecules and 12 $CHCl_3$ molecules. For a large system (300 atoms), we consider non-polarized calculations at Γ-point of the Brillouin zone, used a Gaussian electronic smearing [32]. The stress force and energy convergence criterions are chosen as 0.02 eV/Å and 10^{-4} eV, respectively. The van der Waals interlayer interaction is treated by a semi-empirical DFT-D2 method [33,34].

3. Results and discussion

3.1. Reversible phase transfer of Au@PNIPAM NPs

We fabricate these nanotransporters via biphasic centrifugation to form a plasmonic water droplet floating on the $CHCl_3$ (Fig. 1b-i). The Au NPs are mostly situated at the water/$CHCl_3$ interface due to

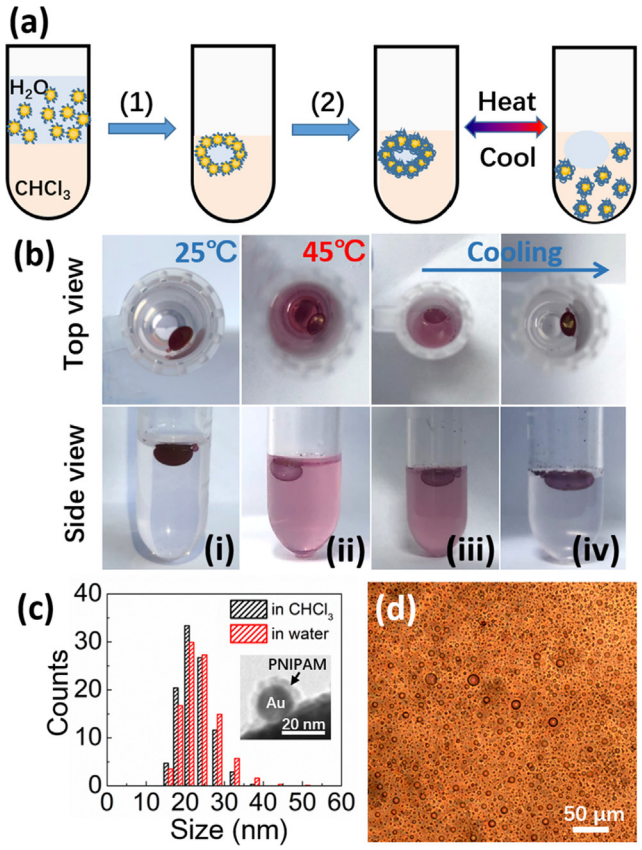

Fig. 1. Reversible phase transfer of Au@PNIPAM NPs between water and $CHCl_3$. (a) Fabrication scheme of the reversible phase transfer system. The mixture of Au@PNIPAM and $CHCl_3$ is 1) centrifuged, followed by discarding large amount of aqueous phase to form a small droplet, and 2) a post-polymerization of PNIPAM at the interface performed to enhance the coating density. (b) Pictures of the reversible phase transfer process of Au/PNIPAM system in one cycle of heating and cooling. (c) Hydrodynamic diameter of Au@PNIPAM NPs in water and $CHCl_3$. The averaged sizes of Au@PNIPAM NPs in water and $CHCl_3$ are 23 ± 1 nm and 22 ± 1 nm, (fitted with Gaussian distribution), respectively. Inset is the TEM image of Au@PNIPAM core-shell NP after post-polymerization. (d) Optical image (transmission) of the plasmonic microemulsion as shown in b-iii).

the centrifugation forces, which overcomes the interfacial energy barrier [35]. However, these Au NPs at interface are not aggregated due to the steric hindrance of PNIPAM chains. Further coating of PNIPAM *via in-situ* polymerization is necessary to enhance its physical entanglement to the Au NPs, which is crucial for the recyclability of Au NPs. This is because without such a post-polymerization, the PNIPAM ligand coating can be easily disassociated from the surface of Au NPs in $CHCl_3$, rendering permanent trapping of Au NPs in $CHCl_3$ phase even if the temperature drops below the LCST (SI-Fig. S4). The $CHCl_3$ phase appears pink red after the temperature rises to 45 °C (Fig. 1b-ii). The particles' hydrodynamic diameter measured in aqueous phase (23 ± 1 nm) is slightly larger than that measured in $CHCl_3$ phase (22 ± 1 nm), which is mainly due to the better swelling of PNIPMA shells in water (Fig. 1c). The post-polymerized PNIPAM shell thickness is ~4 nm as indicated by the TEM image (Inset of Fig. 1c), which agrees with the hydrodynamic diameter. Cooling the temperature back to 25 °C leads to micro-phase separation in $CHCl_3$ with appearance of cloudy pink (Fig. 1b-iii), which however takes a long time (greater than 90 min) to switch back to clearance (Fig. 1b-iv). Microscopic observation of this cloudy mixture shows dispersion of water microdroplets (5–10 μm) containing Au NPs, which is temporally stabilized by PNIPAM (Fig. 1d). As this reverse emulsion is thermodynamically unstable, they tend to merge and migrate to the main water droplet. As a result, the $CHCl_3$ becomes clear again. If the main water droplet is removed before cooling, the hydrophilic Au@PNIPAM NPs have to aggregate in $CHCl_3$ phase to minimize the surface to volume ratio. As such, a redshift of plasmon is observed (SI-Fig. S5). This reversible color switching phenomenon indicates the transfer of Au NPs between $CHCl_3$ and interface (Fig. 1b).

To further characterize its reversibility, we monitor the extinction spectra change of the $CHCl_3$ phase during the phase transfer process (Fig. 2). The plasmon peak at 531 nm emerges in the first 3 mins' heating (as indicated by the red arrows in Fig. 2a), which suggests the Au NPs are gradually diffused into the $CHCl_3$. When the temperature cools down to 25 °C, the $CHCl_3$ phase turns cloudy and the extinction spectra are dominated by the scattering of emulsion, from which we cannot resolve any plasmon peak (as indicated by the blue arrow in Fig. 2a). This cloudiness in $CHCl_3$ phase persists for about 1.5 hr before it disappears (Fig. 2b), which is due to the slow kinetics of de-emulsification. After this de-emulsification, the plasmon peak can be resolved again but with much weaker intensity (SI-Fig. S6), which suggests most of the Au NPs are transferred back to the water/$CHCl_3$ interface. The whole transfer process can be reversible for many times (Fig. 2c, d), but it appears some residue Au NPs are still in $CHCl_3$ phase after each cycle as suggested by the weak intensity in the extinction (Fig. 2c). This residue amount is stable after a few cycles and we take account of this portion of extinction when quantifying the extraction efficiency in later section.

3.2. The mechanism

The change of interfacial energy of Au@PNIPAM NP between water and $CHCl_3$ is crucial for the reversible phase transfer process (Fig. 3a). In the cold state, due to the hydrophilic nature of PNIPAM coating, the Au@PNIPAM NP has a contact angle smaller than 90° at the interface. When the temperature rises above the LCST, the dehydration of PNIPAM chains increases the contact angle between Au@PNIPAM NP and water, and the overall surface tension drags the Au@PNIPAM NP into the $CHCl_3$ phase, leading to phase transfer. When the temperature cools down again, the PNIPAM chains in $CHCl_3$ tend to interact with water molecules that dissolved in $CHCl_3$ via hydrogen bonding, which forms reverse emulsion. It is clear that the water droplets function as the reservoir of water molecules for the reverse emulsification in $CHCl_3$ as no such a reverse emulsion appears if the water droplet is removed before cooling (SI-Fig. S5).

Such reverse emulsification with Au@PNIPAM NPs is not thermodynamically favorable as small droplets tend to merge into bigger ones to reduce their surface to volume ratio. The kinetic stable state however can be achieved with assistance of amphiphilic (macro) molecules and colloids, forming Pickering emulsion [36]. Therefore, the switchable surface hydrophobicity of Au@PNIPAM NPs is critical for such reverse emulsification process [37–39]. Lowering the temperature below the LCST decreases the water contact angle on Au, thus allowing the formation of Pickering emulsion, while increasing the temperature above the LCST results in de-emulsification, which shows clear solution of $CHCl_3$ containing Au NPs (SI-Fig. S7). The Gibbs free energy change of the coalescence process can be calculated as [40]

$$\Delta G_{coal} = 4\pi R_l^2 \gamma_{ow}(2 - 2^{\frac{2}{3}})(\cos\theta(\cos\theta + 2)) \quad (1)$$

where R_l is the radius of the water droplet (~10 μm), γ_{ow} is the interfacial energy between water and $CHCl_3$, θ is the contact angle between water and Au NP. The energy diagram (Fig. 3b) suggests the coalescence is energetically favorable when the contact angle

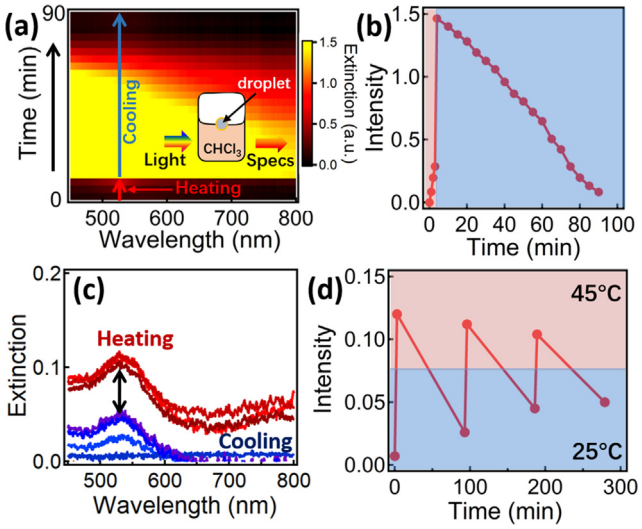

Fig. 2. (a) Extinction spectra of Au NPs in $CHCl_3$ in one cycle of heating and cooling. Inset is the scheme of extinction measurement. (b) Change of extinction intensity (at 531 nm) with time. The light red and blue colors represent the heating and cooling period, respectively. (c) Extinction spectra of Au@PNIPAM NPs in chloroform with 3 cycles of heating and cooling. (d) Change of extinction intensity with time of temperature cycling. (For interpretation of the references to color in this figure legend, the reader is referred to the web version of this article.)

is larger than 90°, accompanied with the releasing of Au NPs in $CHCl_3$, which is supported by our experiment (SI-Fig. S7).

This phase transfer process is powered by phase change of PNIPAM, from which we can calculate the energy efficiency of this process. Suppose the thermal energy raises the temperature around the Au@PNIPAM NP with ΔT of 2 °C across the LCST, which leads to the transfer of Au NP from the interface to oil phase driven by the surface tensions. Thus, the thermal input (Q) and work (W) that transfer the Au NPs from interface to $CHCl_3$ can be calculated with formula

$$Q = (c_{Au}m_{Au} + c_{sol}m_{sol})\Delta T \quad (2)$$

$$W = -\Delta G = -(4\pi r^2\sigma_{Au-O} - 2\pi r^2(\sigma_{Au-W} + \sigma_{Au-O})) \quad (3)$$

where c_{Au} and c_{sol} are the thermal capacity of gold and solvent respectively, m_{Au} and m_{sol} are the mass of gold and solvent layer (~18 nm) [41]. Thus, the energy efficiency (W/Q) of this metallic nanotransporter estimated from these formulas is ~1.4% (see SI for detailed calculation).

3.3. Molecular extraction assisted by Au@PNIPAM NPs

By repeated heating and cooling, the hybrid nanoshuttles transfer back and forth between water/$CHCl_3$ interface and $CHCl_3$ bulk phase, which can be utilized to boost the molecular extraction process. Here we choose R6G as the model molecules for extraction from aqueous phase to $CHCl_3$ phase. As the solubility of R6G molecules in $CHCl_3$ is lower than that in water, the pollution remediation efficiency via conventional solvent extraction is low. The difficulty can be overcome by decreasing the interfacial barrier. Thus, we apply this reversible phase transfer system to help with the extraction process. With cycles of heating and cooling, the R6G molecules steadily increase their concentration in $CHCl_3$ phase as suggested by the increasing intensity of their absorbance (Fig. 4a). In the meanwhile, their absorbance in aqueous phase decreases (Fig. 4b), suggesting the extraction is indeed happening. However, without such metallic nanotransporters, the absorption intensity only slightly increases after the same number of heating and cooling cycles (SI-Fig. S8). This contrast experiment clearly suggests the important role of Au cores for the R6G transportation, which is likely because of their high adsorption for R6G molecules. Such nanoparticle-assisted extraction obviously outperforms traditional solvent extraction method via physical agitation such as shaking and sonication, which only shows absorbance of 0.2 (SI-Fig. S9).

The advantage of this reversible phase transfer system is further augmented by the fact that the metallic nanotransporters can be recovered and reused after cooling and simple separation/purification process (SI-Fig. S10).

3.4. Thermodynamic analysis of the NP assisted extraction process

The whole process of nanoparticle-assisted extraction of R6G can be understood from thermodynamics and kinetics perspective (Fig. 4d). In cold state, the Au@PNIPAM NPs situated at the water/$CHCl_3$ interface adsorb the R6G molecules on their surfaces. When the temperature increases above the LCST, the Au@PNIPAM NPs along with the adsorbed R6G molecules are transferred into the $CHCl_3$ phase. Then the R6G molecules are desorbed from Au NP surfaces and diffuse into the $CHCl_3$ to reach thermodynamic equilibrium. When the temperature cools down, the Au@PNIPAM NPs transfer back to the water/$CHCl_3$ interface for another round of adsorption, transfer and desorption processes.

The reverse emulsification may also promote the extraction process as it increases the interface areas. With cycles of heating and cooling, the R6G molecules are gradually transported into $CHCl_3$ by the Au NPs, which eventually saturates at ~60 μM

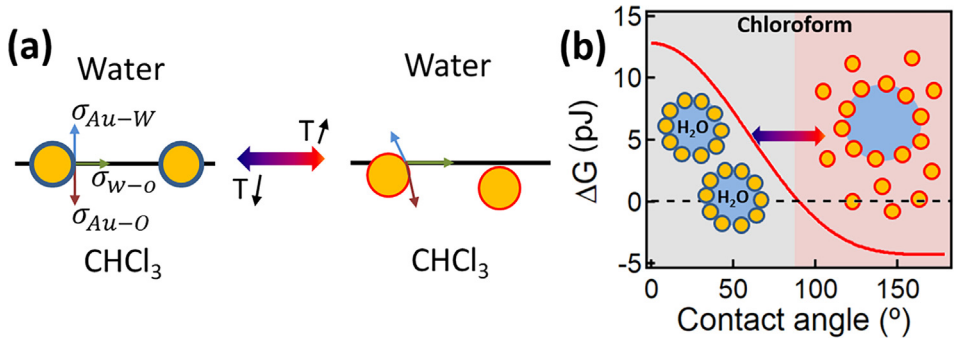

Fig. 3. Mechanism of the nanoparticle phase transfer process and its energy profile analysis. (a) Scheme of the contact angle change at the interface of water, $CHCl_3$ and Au@PNIPAM NPs. At the interface, when the temperature is below the LCST, the contact angle is ~90°. When the temperature rises above the LCST, the three phase contact angle changes, and net surface tension draws the Au@PNIPAM NP into the $CHCl_3$ phase. σ_{W-O}, σ_{Au-W}, and σ_{Au-O} are the interfacial energy between water and $CHCl_3$, gold and water, gold and $CHCl_3$, respectively. (b) Gibbs free energy change of the microdroplet at different contact angles of Au NPs and water. Inset shows the scheme of coalescence of two droplets into one big droplet.

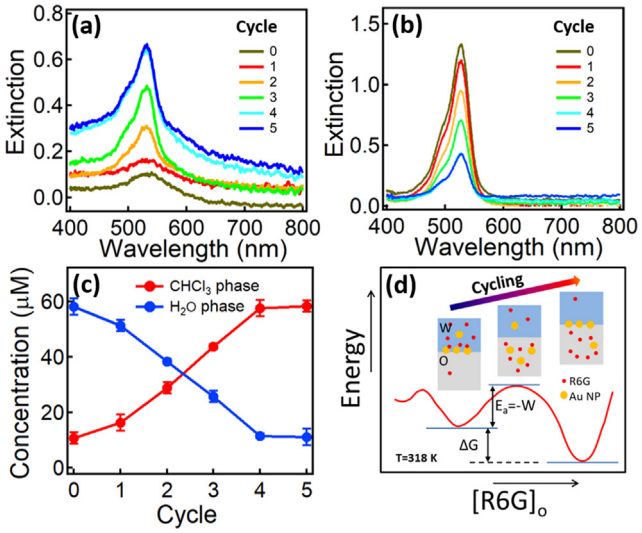

Fig. 4. Au@PNIPAM NPs assisted extraction of R6G molecules. (a, b) Absorption spectra of R6G molecules in $CHCl_3$ and H_2O phases with increasing cycle of heating and cooling. (a) $CHCl_3$ phase (b) H_2O phase. Note: the extinctions of residue Au NPs in $CHCl_3$ are subtracted. (c) The change of R6G concentration in $CHCl_3$ and H_2O phases with the cycle number. (d) Scheme of the nanoparticle-assisted extraction process and Gibbs free energy change.

(Fig. 4c). Note that the initial R6G concentration in water phase is ~6.9 mM, and after normal solvent extraction process, the ideal partition of R6G in $CHCl_3$ can reach above 60 μM. However, due to interfacial barrier between water and $CHCl_3$ [35], it is kinetically unfavorable to reach such concentration. Such an interfacial barrier can be overcome by the phase transfer of Au@PNIPAM NPs, which 'catalyzes' the extraction process (Fig. 4d).

The free energy change of the R6G extraction can be calculated with $\Delta G = -RT\ln(\frac{K'}{K})$, where K and K′ are the distribution coefficient ($\frac{[R6G]_O}{[R6G]_W}$) of R6G without and with metallic nanotransporters. The Gibbs free energy change of this extraction is −14.6 kJ/mol, which is thermodynamically favorable but kinetically unfavorable as it has to overcome the interfacial energy barrier (E_a) (Fig. 4d). With the work of R6G adsorption, Au NPs transportation and emulsification, such an activation energy barrier can be satisfied, which is followed by desorption and diffusion of R6G in $CHCl_3$.

This energy analysis is also supported qualitatively by the *ab initio* density functional theory calculations (see numerical results shown in Fig. 5). Clearly, the energy of R6G in $CHCl_3$ phase (State-I) shows lower energy level ($\Delta E = -1.65$eV) than that in water phase (State-III), which suggests it is indeed thermodynamically favorable. The energy barrier (E_a') for this extraction is ~4 eV (Fig. 5b), which is approximately the work done by the Au NP transportation.

4. Conclusions

In summary, we demonstrate a novel concept of molecular extraction with the assistance of nanotransporters. These nanotransporters are made of Au@PNIPAM NPs, which transfer between the water/$CHCl_3$ interface and $CHCl_3$ phase with the assistance of PNIPAM phase change. With repeated transportation, the cargo molecules (R6G) can be consecutively delivered from aqueous phase to $CHCl_3$ phase, leading to much higher extraction efficiency (5 times higher than that without nanotransporters). And the energy efficiency for the nanotransportation is ~1.4%. We further reveal the underlying mechanism from energy perspective. Unlike previous strategy of nanoparticle-assisted extraction [9,10], this nanotransportation system is more efficient and eco-friendly with features of excellent reversibility and recyclability. For future development, this nanotransportation system not only can be applied for pollution treatment, but also can be used as a new type of nanomachines that transport and deliver drugs into the desired locations of the organs and tissues via hydrophobic interactions [42,43] at the via hydrophobic interactions [44,45].

CRediT Author statement

Chi Zhang: Methodology, Validation, Formal analysis, Investigation, Data curation, Writing - original draft, Visualization,

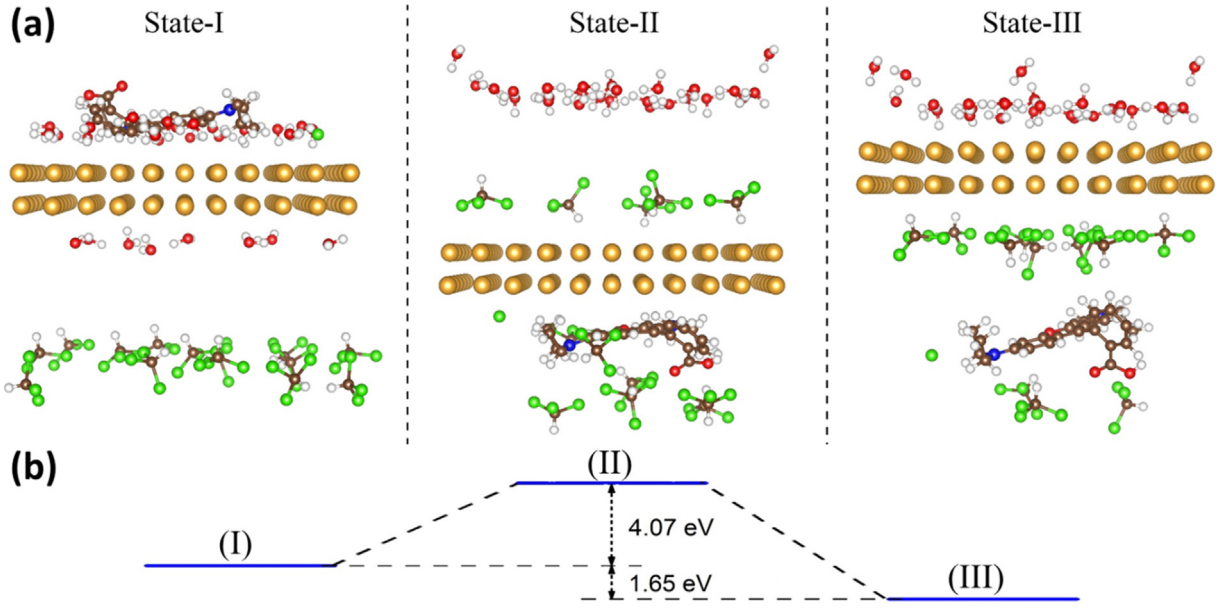

Fig. 5. Energy calculations of the nanotransportation system at different states. (a) Side views of the R6G/Au/H_2O/$CHCl_3$ system: (I) R6G/Au in water phase, (II) R6G/Au in $CHCl_3$ phase, and (III) Au back at the interface but R6G in the $CHCl_3$ phase. Brown, red, green, white and yellow dots represent carbon, oxygen, chlorine, hydrogen and gold atoms. (b) Is the energy level of these three states. (For interpretation of the references to color in this figure legend, the reader is referred to the web version of this article.)

Writing - review & editing. **Fangfang Deng:** Methodology, Validation, Investigation, Writing - review & editing. **Wenqi Xiong:** Methodology, Software, Validation, Formal analysis, Investigation, Data curation. **Xujie Wang**: Validation, Formal analysis. **Shengjun Yuan:** Supervision, Resources, Writing-review & editing. **Tao Ding:** Conceptualization, Methodology, Formal analysis, Writing - original draft, Supervision, Resources, Funding acquisition, Project administration, Writing - review & editing.

Declaration of Competing Interest

The authors declare that they have no known competing financial interests or personal relationships that could have appeared to influence the work reported in this paper.

Acknowledgements

This research is supported by the National Natural Science Foundation of China (NSFC, 21703160, 11974265), Wuhan Science and Technology Project (2019010701011420) and Fundamental Research Funds for the Central Universities (2042018kf0254, 2042018kf0038). We thank the support of Supercomputing Center of Wuhan University for the numerical calculations in this paper.

Appendix A. Supplementary material

Supplementary data to this article can be found online at https://doi.org/10.1016/j.jcis.2020.10.008.

References

[1] R.L.P. Thomas, K. Sherwood, Absorption and Extraction, second ed., McGraw-Hill Education, New York, 1952.
[2] G.R. Choppin, A. Morgenstern, Thermodynamics of solvent extraction, Solvent Extr. Ion. Exc 18 (6) (2000) 1029–1049.
[3] J.A. Asenjo, B.A. Andrews, Aqueous two-phase systems for protein separation: a perspective, J. Chromatogr. A 1218 (49) (2011) 8826–8835.
[4] M. Iqbal, Y. Tao, S. Xie, Y. Zhu, D. Chen, X. Wang, L. Huang, D. Peng, A. Sattar, M. A.B. Shabbir, H.I. Hussain, S. Ahmed, Z. Yuan, Aqueous two-phase system (ATPS): an overview and advances in its applications, Biol. Proced. Online. 18 (1) (2016) 18.
[5] S.R. Chia, M.S.Y. Tang, Y.H. Chow, C.W. Ooi, K. Rambabu, L. Zhu, P.L. Show, Recent developments of reverse micellar techniques for lysozyme, bovine serum albumin, and bromelain extraction, Mol. Biotechnol. 61 (10) (2019) 715–724.
[6] M.J. Pires, M.R. Aires-Barros, J.M.S. Cabral, Liquid−liquid extraction of proteins with reversed micelles, Biotechnol. Prog. 12 (3) (1996) 290–301.
[7] G. Brunner, Applications of supercritical fluids, Annu. Rev. Chem. Biomol 1 (1) (2010) 321–342.
[8] C.A. Eckert, B.L. Knutson, P.G. Debenedetti, Supercritical fluids as solvents for chemical and materials processing, Nature 383 (6598) (1996) 313–318.
[9] L. Reinišová, S. Hermanová, M. Pumera, Micro/nanomachines: what is needed for them to become a real force in cancer therapy?, Nanoscale 11 (14) (2019) 6519–6532
[10] Y. Zhang, K. Yuan, L. Zhang, Micro/nanomachines: from functionalization to sensing and removal, Adv. Mater. Technol. 4 (4) (2019) 1800636.
[11] P. Amani, M. Amani, G. Ahmadi, O. Mahian, S. Wongwises, A critical review on the use of nanoparticles in liquid-liquid extraction, Chem. Eng. Sci. 183 (2018) 148–176.
[12] Z. Shi, H. Lee, Dispersive liquid-liquid microextraction coupled with dispersive μ-solid-phase extraction for the fast determination of polycyclic aromatic hydrocarbons in environmental water samples, Anal. Chem. 82 (4) (2010) 1540–1545.
[13] M. Safari, Y. Yamini, E. Tahmasebi, B. Ebrahimpour, Magnetic nanoparticle assisted supramolecular solvent extraction of triazine herbicides prior to their determination by HPLC with UV detection, Microchimi. Acta 183 (2015).
[14] G. Yang, W.-S. Chang, D.T. Hallinan, A convenient phase transfer protocol to functionalize gold nanoparticles with short alkylamine ligands, J. Colloid Interf. Sci 460 (2015) 164–172.
[15] K.S. Mayya, F. Caruso, Phase transfer of surface-modified gold nanoparticles by hydrophobization with alkylamines, Langmuir 19 (17) (2003) 6987–6993.
[16] L. Peng, M. You, C. Wu, D. Han, I. Öçsoy, T. Chen, Z. Chen, W. Tan, Reversible phase transfer of nanoparticles based on photoswitchable host-guest chemistry, ACS Nano 8 (3) (2014) 2555–2561.
[17] J.B. ten Hove, L.M.I. Schijven, J. Wang, A.H. Velders, Size-controlled and water-soluble gold nanoparticles using UV-induced ligand exchange and phase transfer, Chem. Commun. 54 (95) (2018) 13355–13358.
[18] V.A. Turek, L.N. Elliott, A.I.I. Tyler, A. Demetriadou, J. Paget, M.P. Cecchini, A.R. Kucernak, A.A. Kornyshev, J.B. Edel, Self-assembly and applications of ultraconcentrated nanoparticle solutions, ACS Nano 7 (10) (2013) 8753–8759.
[19] G.-T. Wei, Z. Yang, C.-Y. Lee, H.-Y. Yang, C.R.C. Wang, Aqueous−organic phase transfer of gold nanoparticles and gold nanorods using an ionic liquid, J. Am. Chem. Soc. 126 (16) (2004) 5036–5037.
[20] A.M. Alkilany, A.C. Caravana, M.A. Hamaly, K.T. Lerner, L.B. Thompson, Phase transfer of citrate stabilized gold nanoparticles using nonspecifically adsorbed polymers, J. Colloid Interf. Sci 461 (2016) 39–44.
[21] M. Karg, N. Schelero, C. Oppel, M. Gradzielski, T. Hellweg, R. von Klitzing, Versatile phase transfer of gold nanoparticles from aqueous media to different organic media, Chem. Eur. J. 17 (16) (2011) 4648–4654.
[22] T. Ding, A.W. Rudrum, L.O. Herrmann, V. Turek, J.J. Baumberg, Polymer-assisted self-assembly of gold nanoparticle monolayers and their dynamical switching, Nanoscale 8 (35) (2016) 15864–15869.
[23] R. Pelton, Poly(N-isopropylacrylamide) (PNIPAM) is never hydrophobic, J. Colloid Interf. Sci 348 (2) (2010) 673–674.
[24] T. Honold, D. Skrybeck, K.G. Wagner, M. Karg, Fully reversible quantitative phase transfer of gold nanoparticles using bifunctional PNIPAM ligands, Langmuir 33 (1) (2017) 253–261.
[25] V.A. Turek, S. Cormier, B. Sierra-Martin, U.F. Keyser, T. Ding, J.J. Baumberg, The crucial role of charge in thermoresponsive-polymer-assisted reversible dis/assembly of gold nanoparticles, Adv. Opt. Mater. 6 (8) (2018) 1701270.
[26] T. Ding, J.J. Baumberg, Thermo-responsive plasmonic systems: old materials with new applications, Nanoscale Adv. 2 (4) (2020) 1410–1416.
[27] W. Bao, J. Wang, Q. Wang, D. O'Hare, Y. Wan, Layered double hydroxide nanotransporter for molecule delivery to intact plant cells, Sci. Rep. 6 (1) (2016) 26738.
[28] M. Hemmati, M. Rajabi, A. Asghari, Magnetic nanoparticle based solid-phase extraction of heavy metal ions: a review on recent advances, Microchim. Acta 185 (3) (2018) 160.
[29] H.D. Jang, H. Kim, H. Chang, J. Kim, K.M. Roh, J.-H. Choi, B.-G. Cho, E. Park, H. Kim, J. Luo, J. Huang, Aerosol-assisted extraction of silicon nanoparticles from wafer slicing waste for lithium ion batteries, Sci. Rep. 5 (2015) 9431.
[30] G. Qing, X. Zhao, N. Gong, J. Chen, X. Li, Y. Gan, Y. Wang, Z. Zhang, Y. Zhang, W. Guo, Y. Luo, X.-J. Liang, Thermo-responsive triple-function nanotransporter for efficient chemo-photothermal therapy of multidrug-resistant bacterial infection, Nat. Commun. 10 (1) (2019) 4336.
[31] J. Turkevich, P.C. Stevenson, J. Hillier, A study of the nucleation and growth processes in the synthesis of colloidal gold, Discuss. Faraday Soc. 11 (1951) 55–75.
[32] F. Deng, Y. Wang, X. Lu, T. Ding, Probing hidden colloidal transitions with the assistance of surface plasmons, PCCP 21 (28) (2019) 15742–15746.
[33] J.P. Perdew, K. Burke, M. Ernzerhof, Generalized gradient approximation made simple, Phys. Rev. Lett. 77 (18) (1996) 3865–3868.
[34] H.J. Monkhorst, J.D. Pack, Special points for brillouin-zone integrations, Phys. Rev. B 13 (12) (1976) 5188–5192.
[35] S. Grimme, Semiempirical GGA-type density functional constructed with a long-range dispersion correction, J. Comput. Chem. 27 (15) (2006) 1787–1799.
[36] T. Kerber, M. Sierka, J. Sauer, Application of semiempirical long-range dispersion corrections to periodic systems in density functional theory, J. Comput. Chem. 29 (13) (2008) 2088–2097.
[37] V.A. Turek, M.P. Cecchini, J. Paget, A.R. Kucernak, A.A. Kornyshev, J.B. Edel, Plasmonic ruler at the liquid-liquid interface, ACS Nano 6 (9) (2012) 7789–7799.
[38] J. Wu, G.-H. Ma, Recent studies of Pickering emulsions: particles make the difference, Small 12 (34) (2016) 4633–4648.
[39] B.P. Binks, R. Murakami, S.P. Armes, S. Fujii, Temperature-induced inversion of nanoparticle-stabilized emulsions, Angew. Chem. Int. Ed. 44 (30) (2005) 4795–4798.
[40] J.T. Tang, P.J. Quinlan, K.C. Tam, Stimuli-responsive Pickering emulsions: recent advances and potential applications, Soft Matter 11 (18) (2015) 3512–3529.
[41] Y. Horiguchi, H. Kawakita, K. Ohto, S. Morisada, Temperature-responsive Pickering foams stabilized by poly(N-isopropylacrylamide) nanogels, Adv. Powder Technol. 29 (2) (2018) 266–272.
[42] B.P. Binks, T.S. Horozov, Colloidal Particles at Liquid Interfaces, first ed., Cambridge University Press, Cambridge, 2006.
[43] F. Deng, J. Feng, T. Ding, Chemoplasmonic oscillation: a chemomechanical energy transducer, ACS Appl. Mater. Inter. 11 (45) (2019) 42580–42585.
[44] C.D. Montemagno, Nanomachines: a roadmap for realizing the vision, J. Nanopart. Res. 3 (1) (2001) 1–3.
[45] T. Ding, V.K. Valev, A.R. Salmon, C.J. Forman, S.K. Smoukov, O.A. Scherman, D. Frenkel, J.J. Baumberg, Light-induced actuating nanotransducers, PNAS 113 (20) (2016) 5503–5507.